

Supporting Information

Dependence on size of supported Rh nanoclusters for CO adsorption

Ting-Chieh Hung^a, Ting-Wei Liao^a, Zhen-He Liao^a, Po-Wei Hsu^a, Pei-Yang Cai^a, Wen-Hua Lu^b, Jeng-Han Wang^{b,*} and Meng-Fan Luo^{a,*}

^aDepartment of Physics, National Central University, 300 Zhongda Road, Zhongli 32001, Taiwan

^bDepartment of Chemistry, National Taiwan Normal University, Taipei, Taiwan

Corresponding Author

*E-mail: mfl28@phy.ncu.edu.tw (M.F. Luo); jenghan@ntnu.edu.tw (J. H. Wang)

Fig. 1S(a) and (b) show CO IRAS spectra for 0.3 ML and 1.1 ML Rh clusters on Al₂O₃/NiAl(100) exposed to 2.0 L CO at 100 K and annealed to selected temperatures. Both series of spectra show a similar trend that with increasing temperature, the CO lines attenuated and shifted negatively to smaller wavenumbers. The attenuation indicates desorption of CO and the negative shift of the wavenumber is ascribed to weakened CO-CO interactions because of decreased CO on the surface. The wavenumber shift with the temperature was also observed for CO on supported Pt clusters.¹ Both series of spectra show a dramatic change in the wavenumber and intensity at 400 K, indicating a significant desorption of CO. However, a careful analysis of the intensity suggests different onset temperatures of CO desorption for CO on 0.3 and 1.1 ML clusters. Fig. 1S(c) and (d) plot respectively the integrated intensities of CO lines from CO on 0.3 ML and 1.1 ML clusters, as a function of temperature. The intensities are normalized to the ones at 100 K. It is clear

that CO on 0.3 ML clusters began to decrease at lower temperature. At 300 K, the intensity on 0.3 ML clusters decreased by more than 20 %, whereas that on 1.1 ML clusters by only 10 %. The result is consistent with the TPD experiments that on smaller clusters (smaller Rh coverages) the CO desorption begins at lower temperature.

Fig. S2 shows STM image for 2.5 ML Rh on Al₂O₃/NiAl(100), an example of surface morphologies for 2.0 - 4.0 ML Rh on Al₂O₃/NiAl(100). At this coverage, Rh clusters coalesced heavily, as exemplified in the circled area, and almost covered the entire oxide surface; isolated clusters as those in Fig. 1(a)-(c) were few. Such morphological features were generally observed in the coverage regime 2.0 - 4.0 ML Rh.

Fig. S3 compares the CO TPD spectra from 2.0 L CO adsorbed on 1.6, 2.3, 3.0 and 4.0 ML Rh clusters on Al₂O₃/NiAl(100). The comparison shows that the spectra altered gradually with the coverage; there was no clear threshold coverage for the alternation. Notably, the onset temperature increased continuously with the coverage. The coverage regime 2.0 – 4.0 ML was not investigated in the present study because the clusters coalesced heavily in the regime and thus the properties are not readily associated with typically defined sizes.

Fig. S4 shows Bader charge as a function of surface coverage (θ) of CO on **Rh(100)**, **Rh(100)_E** surfaces and **Rh_C** cluster. The more negatively charged CO indicates that OC-Rh bond is more ionic and E_{ads} of CO is greater. Accordingly, CO has the strongest E_{ads} on **Rh_C** and its charge is the most negative. The decrease of the ionicity of CO with increasing θ supports that E_{ads} is reduced at higher CO surface coverage.

Fig. S5 compares density-of-states (DOS) of surface CO at high (dash lines) and low (solid

lines) coverages on **Rh(100)**, **Rh(100)_E** surfaces and **Rh_C** cluster. (a), (c) and (e) are carbon *p* bands of surface CO, and (b), (d) and (f) are oxygen *p* bands of surface CO. DOS becomes broader and has greater anti-binding distribution above the Fermi level at higher CO coverage, demonstrated as the circled regions in the figures. The comparison indicates that CO adsorption is relatively weaker at higher CO coverage on the two surfaces and the cluster.

Table S1(a) compares the adsorption energies calculated at the GGA-PW91 level and at the GGA-PBE level with vdW-DF correlation functional. The comparison suggests that the GGA-PBE with vdW-DF correlation functional can resolve the CO puzzle.² The top site becomes the most favored one on either Rh surface or cluster. The CO adsorption on **Rh_C** remains stronger than that on **Rh(100)_E** and **Rh(100)**. Table S1(b) shows averaged adsorption energies of CO at the GGA-PW91 level at different coverages on both Rh surfaces and the cluster. The adsorption energy decreases slower as the CO coverage increases on **Rh_C** than those on **Rh(100)_E** and **Rh(100)** surfaces.

References

- (1) C.-S. Chao, Y.-D. Li, B.-W. Hsu, W.-R. Lin, H.-C. Hsu, T.-C. Hung, C.-C. Wang, M.-F. Luo, *J. Phys. Chem. C*, 2013, **117**, 5667.
- (2) P. J. Feibelman, B. Hammer, J. K. Nørskov, F. Wagner, M. Scheffler, R. Stumpf, R. Watwe, J. Dumesic, *J. Phys. Chem. B* 2001, **105**, 4018

Figures and captions

Fig. S1

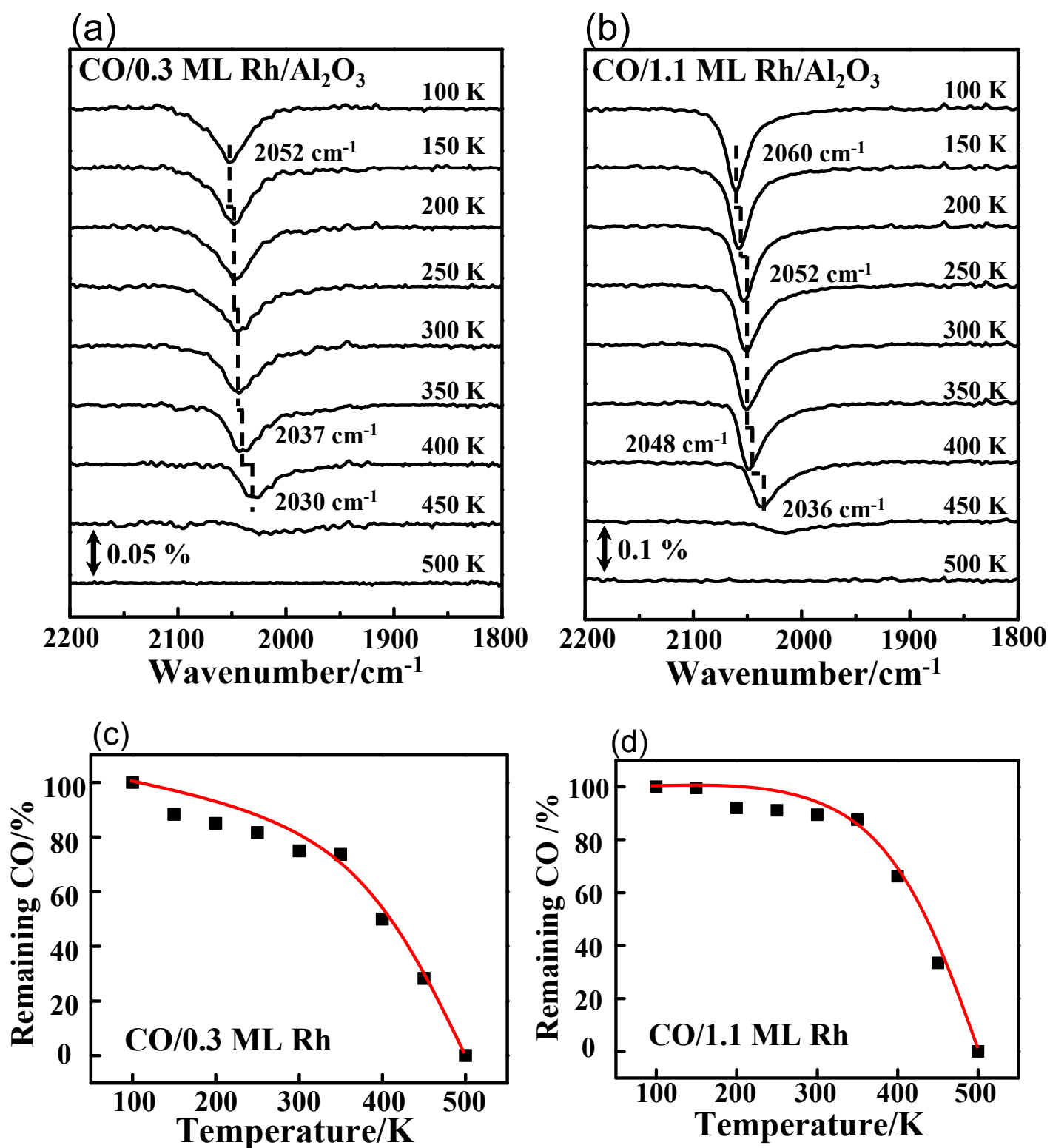


Fig. S1 CO IRAS spectra for 2.0 L CO

adsorbed on (a) 0.3 ML and (b) 1.1 ML Rh clusters on Al₂O₃/NiAl(100) at 100 K and

annealed to selected temperatures; plots of the integrated intensity of the absorption line as a function of temperature from (c) 0.3 ML and (d) 1.1 ML Rh clusters. The intensities in (c) and (d) are normalized to the ones at 100 K and the red lines are drawn to guide the eye. The Rh clusters were formed at 300 K and each spectrum was recorded when the surface was cooled to 100 K after annealing to the indicated temperature.

Fig. S2

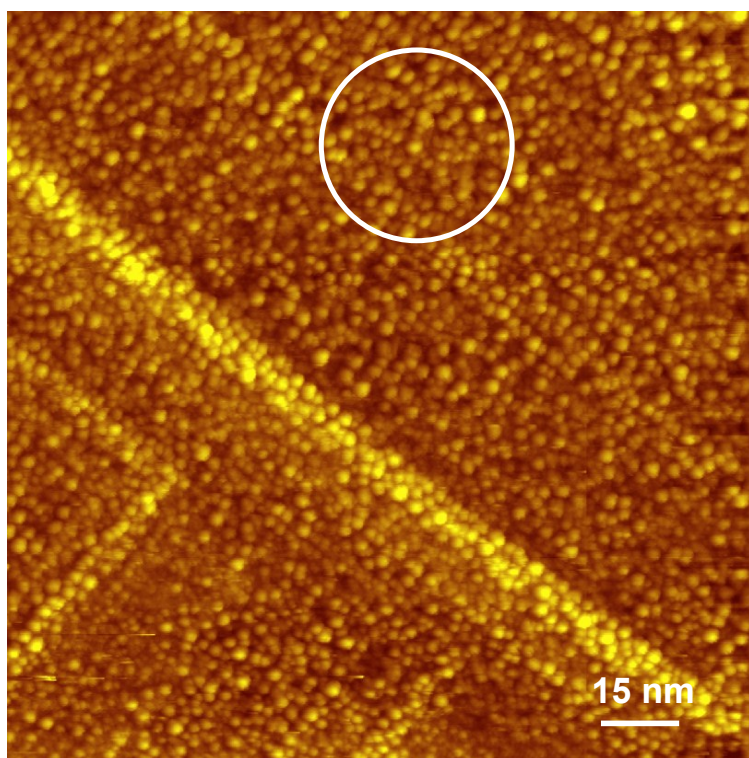


Fig. S2 STM image showing 2.5 ML Rh deposited on a thin film of $\text{Al}_2\text{O}_3/\text{NiAl}(100)$ at 300 K. The circled area shows that the clusters coalesced heavily.

Fig. S3

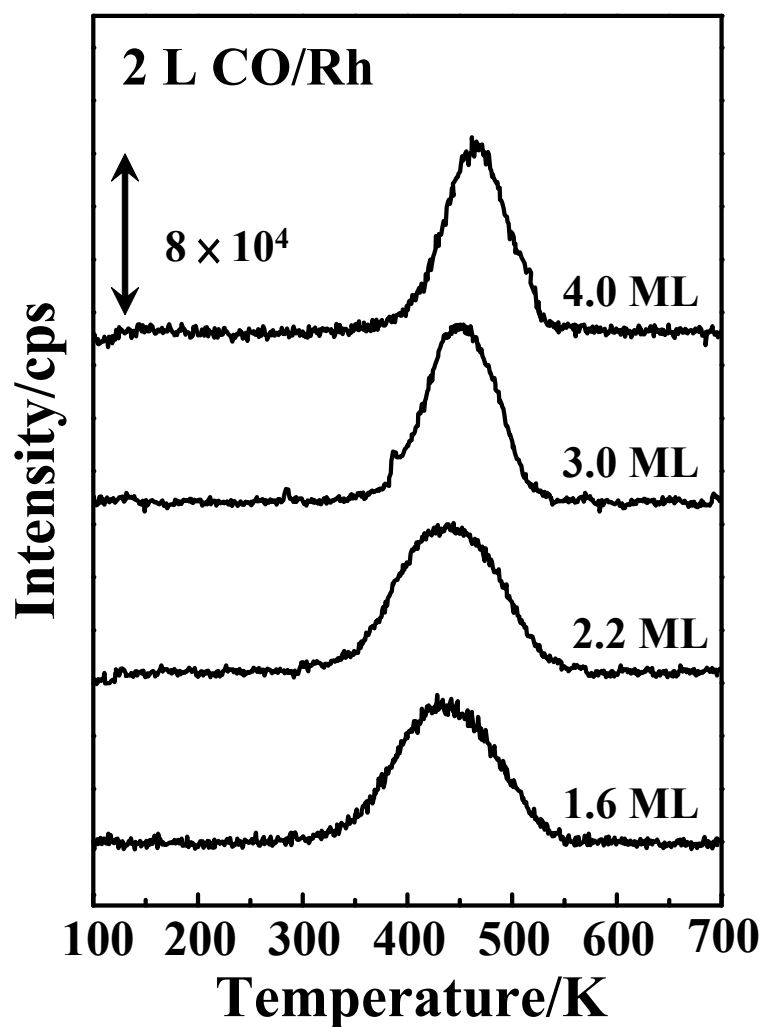


Fig. S3 CO TPD spectra for 2.0 L CO adsorbed on 1.6, 2.3, 3.0 and 4.0 ML Rh clusters on $\text{Al}_2\text{O}_3/\text{NiAl}(100)$. Rh was deposited at 300 K and CO was adsorbed at 100 K.

Fig. S4

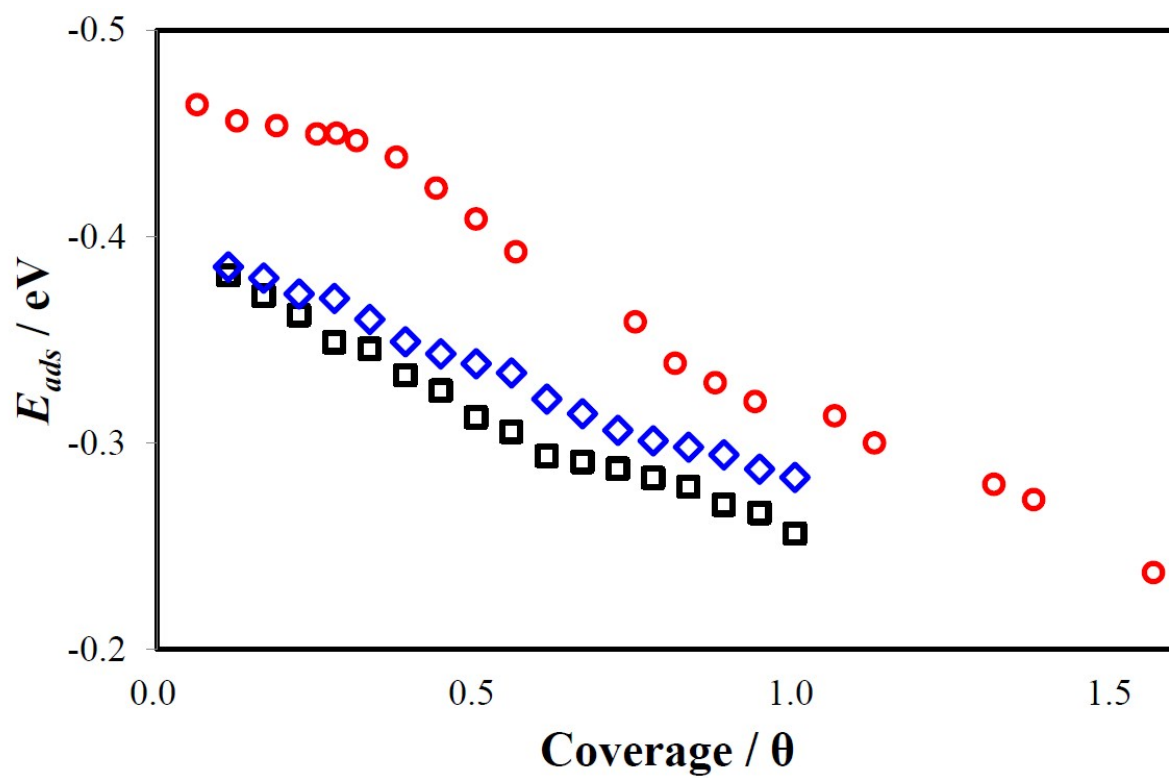


Fig. S4 Bader charge as a function of surface coverage (θ) of CO on **Rh(100)** and **Rh(100)_E** surfaces and **Rh_C** cluster, in black, blue and red symbols, respectively.

Fig. S5

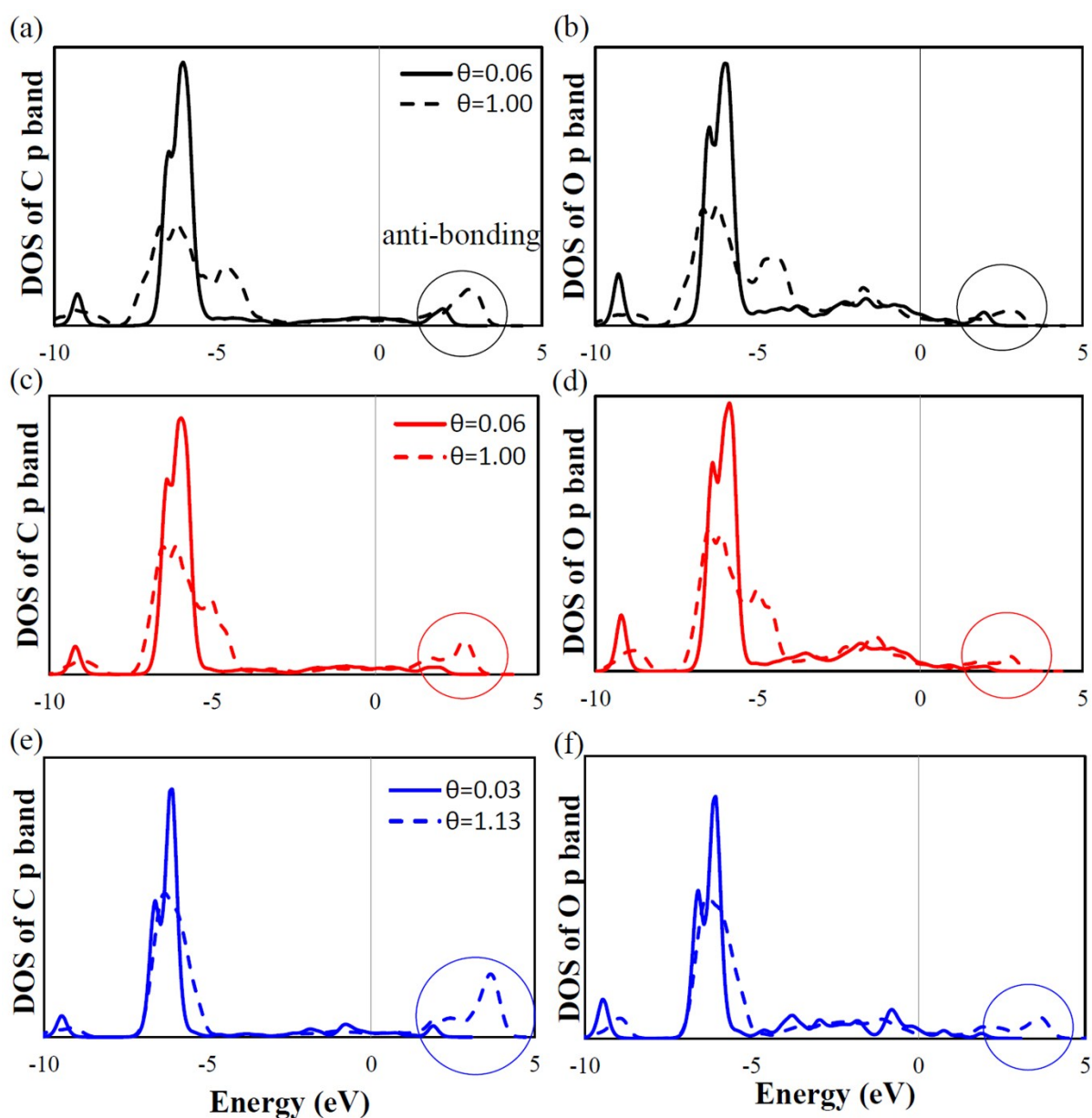


Fig. S5 comparison of DOS of surface CO at high (dash lines) and low (solid lines) coverages on **Rh(100)**, **Rh(100)_E** surfaces and **Rh_C** cluster. (a) and (b) are *p* bands of C and O respectively of surface CO on **Rh(100)** surface; (c) and (d) are *p* bands of C and O respectively of surface CO on **Rh(100)_E** surface; (e) and (f) are *p* bands of C and O respectively of surface CO on **Rh_C** cluster. The Fermi levels are drawn in the figures in solid lines at energy zero. The anti-bonding distributions above the Fermi level are circled in the figures.

Table S1. (a) Adsorption energies of CO at the GGA-PW91 level (in eV) on top, bridge and four-fold-hollow sites on **Rh(100)** and **Rh(100)_E**, and on top, bridge, four-fold-hollow and three-fold-hollow sites on **Rh_C**. Adsorption energies computed at the GGA-PBE level with vdW-DF correlation functional are listed in the parentheses. (b) Averaged adsorption energies of CO at the GGA-PW91 level at different coverages on both surfaces and the cluster.

(a)	Rh(100)	Rh(100)_E	Rh_C	
Top	-1.84 (-2.14)	-2.02 (-2.35)	-2.23 (-2.58)	
Bridge	-1.99 (-2.05)	-2.17 (-2.20)	-2.35 (-2.22)	
Four-fold-hollow	-1.88 (-1.92)	-2.06 (-2.06)	-2.45 (-2.45)	
Three-fold-hollow			-2.24 (-2.14)	

(b)	Rh(100)	Rh(100)_E	Rh_C	
$\theta = 0.06$	-1.99 ~ -1.84	-2.17 ~ -2.02	$\theta = 0.03$	-2.45 ~ -2.24
$\theta = 0.11$	-1.99	-2.17	$\theta = 0.06$	-2.26
$\theta = 0.17$	-1.99	-2.17	$\theta = 0.13$	-2.20
$\theta = 0.22$	-1.99	-2.15	$\theta = 0.19$	-2.18
$\theta = 0.28$	-1.98	-2.14	$\theta = 0.25$	-2.16
$\theta = 0.33$	-1.98	-2.13	$\theta = 0.31$	-2.15
$\theta = 0.39$	-1.95	-2.12	$\theta = 0.38$	-2.13
$\theta = 0.44$	-1.93	-2.11	$\theta = 0.44$	-2.12
$\theta = 0.50$	-1.90	-2.10	$\theta = 0.50$	-2.10
$\theta = 0.56$	-1.89	-2.07	$\theta = 0.56$	-2.07
$\theta = 0.61$	-1.87	-2.02	$\theta = 0.75$	-2.02
$\theta = 0.67$	-1.85	-1.98	$\theta = 0.80$	-2.00
$\theta = 0.72$	-1.84	-1.96	$\theta = 0.88$	-1.98
$\theta = 0.78$	-1.80	-1.93	$\theta = 0.94$	-1.96
$\theta = 0.83$	-1.72	-1.90	$\theta = 1.06$	-1.94
$\theta = 0.89$	-1.69	-1.87	$\theta = 1.13$	-1.90
$\theta = 0.94$	-1.67	-1.84	$\theta = 1.31$	-1.75
$\theta = 1.00$	-1.60	-1.81	$\theta = 1.38$	-1.68
			$\theta = 1.56$	-1.52

